Energy & Buildings 298 (2023) 113517

Contents lists available at ScienceDirect

Energy & Buildings

journal homepage: www.elsevier.com/locate/enb

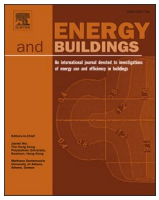

Optical interference coatings for coloured building integrated photovoltaic modules: Predicting and optimising visual properties and efficiency

Arne Røyset [a], Tore Kolås [a,*], Ørnulf Nordseth [b], Chang Chuan You [b]

[a] SINTEF Industry, NO-7465 Trondheim, Norway
[b] Institute for Energy Technology (IFE), NO-2027 Kjeller, Norway

ARTICLE INFO

Keywords:
Thin films
Optical interference
Interference coatings
Colour
Visual appearance
Efficiency
Solar cell
Photovoltaic module
Building integrated photovoltaics
BIPV

ABSTRACT

The presented work is focusing on optical interference coatings on the back side of the front glass for crystalline silicon-based photovoltaic modules. We present results on how such coatings can be designed to obtain desired visual properties combined with a limited loss in power conversion efficiency. This colouring technology may therefore be very attractive for building integrated photovoltaics. Coating design parameters such as number of layers, design wavelength, layer thicknesses, and layer refractive indices affect both the visual appearance parameters and the efficiency. Important colour parameters are lightness, chroma, and hue, and we demonstrate how these colour parameters are influenced by the design parameters of the optical interference coating.

Using optical interference coatings to create colours results in colours that are dependent on the observation angle. We have introduced a new parameter for quantification of angular colour dependence. Our results show that the angular colour dependence can be reduced by increasing the refractive indices of the interference coating.

For many building projects it may be highly desired to combine high power conversion efficiency with certain visual properties. The results from our work also indicate some of the possibilities and challenges in this regard.

1. Introduction

Solar photovoltaics (PV) is the fastest growing energy technology worldwide, with respect to installed electric power capacity. A forecast by the International Energy Agency [1] predicts that the cumulative power capacity of solar PV will surpass hydropower in 2024, surpass natural gas in 2026, and surpass coal in 2027. This will make solar PV the number one technology in the world in 2027 in terms of installed electric power capacity. Distributed solar PV, such as building integrated photovoltaics (BIPV) is expected to account for almost half of the annual additions in capacity within solar PV. In the most optimistic forecast annual additions in distributed PV applications reach almost 170 GW by 2027 [1].

A significant advantage of BIPV is that it produces on-site renewable energy without requiring additional land area. However, when PV modules are utilised as building elements, aesthetic aspects become highly important in addition to the energy performance [2]. In order to meet the aesthetic requirements, coloured PV modules have been manufactured and applied in various types of buildings. Adding colour to an opaque black PV module requires that light is reflected from the module. Increased reflectance will reduce the photon flux available for current generation and thus reduce the electricity generation. Any coloured PV module with a given lightness and chroma will therefore be associated with a loss in electricity generation, as compared to a black module. The theoretical minimum limits for this loss in electricity generation was discussed by Røyset et al., [3] and Halme et al., [4]. In those papers, the assumption was that available photons are used either to generate colour or to generate electricity. In practise however, depending on the colouring technique, the losses associated with colouring may be much larger due to undesired absorption of photons by the materials used to generate colours.

Several different technologies have been applied for adding colour to PV modules [5-7]. One of the frequently reported techniques is the use of single or multilayer thin films on the surface of the solar cell, that introduce spectrally selective reflectance due to constructive interference [8-14]. A main benefit of such interference coatings for colouring of

Abbreviations: ARC, anti-reflection coating; BIPV, building integrated photovoltaics; CIE, Commission Internationale de l'Éclairage; CPI, colour performance index; EVA, ethylene-vinyl acetate; IQE, internal quantum efficiency; NIR, near infrared; PCE, power conversion efficiency.

* Corresponding author.
E-mail address: tore.kolas@sintef.no (T. Kolås).

https://doi.org/10.1016/j.enbuild.2023.113517
Received 30 June 2023; Received in revised form 17 August 2023; Accepted 1 September 2023
Available online 4 September 2023

PV modules is that the thin films used to generate colour absorb very few photons. Most photons are either reflected, and may contribute to the colour appearance, or transmitted and contribute to the electricity generation. Coloured modules based on interference coatings may therefore potentially be very efficient, with losses close to the theoretical minimum limits, provided that the reflectance of the interference coatings in the near infrared (NIR) region can be kept at a low level. One challenge of applying such multi-layer coatings on the front surface of the solar cell is that it most likely will affect other steps of the cell fabrication process, including the surface passivation and metal contacting processes for the front side. This implies that a specific colour might require several unique process steps that will all need to be optimized to ensure high electrical performance for the solar cell. In addition, conventional crystalline silicon solar cells typically have a textured front surface that efficiently traps the incoming photons, e.g., random pyramids or high aspect ratio trenches (black silicon). Such geometric shapes result in a low optical reflection (few photons are escaping), which implies that colours with high lightness and saturation are difficult to obtain.

Interference coatings may also be applied to other surfaces in the PV module, including the surfaces of the front glass. In this case, the incoming light can be manipulated before it reaches the textured surface of the solar cell. Thus, applying the interference coatings to the front glass facilitates a wide choice of colours and provides flexibility for the module producers, since the solar cell design does not need to be altered.

Several studies have focused on interference coatings applied to the front glass of PV modules [15-21]. However, a systematic study of design options and design criteria has been lacking in the literature.

In the presented work we have focused our attention on interference coatings applied on the back surface of the front glass. The important design parameters for the interference coatings are the number of layers, design wavelength, layer thicknesses, and refractive indices. This results in a large design freedom and a wide variation in the reflectance spectra and colours that can be obtained. However, the same coating design parameters also affect the obtained power conversion efficiency for the PV module, hereafter referred to as efficiency, and the range of colour parameters that can be obtained within a given efficiency requirement is therefore limited.

In this paper, we analyse the relationship between the lightness and chroma of the colour and the efficiency loss due to the colouring, using numerical modelling. The validity of the simulation model has been verified for a given set of coating design parameters by comparing simulated reflectance curves to measured reflectance curves for experimental samples that were fabricated. We present novel design guidelines on how the coating design parameters affect the trade-offs between desired visual properties and high efficiency. We further investigate the angular dependence of interference colours, and how the angular dependence is affected by the design parameters. We analyse how a requirement on low angular colour dependence can set limitations to the range of achievable colours, and how low angular colour dependence and high efficiency may also be contradictory requirements. We have not found a comprehensive analysis like this in the literature and believe our results can provide useful insights into how thin film interference can be used to tailor-make PV modules that are both visually attractive and at the same time provide high efficiency.

2. Materials and methods

We are here considering interference coatings on the back side of the front glass for silicon-based PV modules. The calculation of colour parameters and estimation of efficiency loss for such PV modules is based on the same approach that we introduced and discussed in an earlier paper [3]. As described by Røyset et al., in [3], the applied approach considers the following three factors:

- The human perception of colour (lightness, chroma, and hue).
- The internal quantum efficiency characteristics of an idealised silicon solar cell.
- The solar irradiance spectrum at the surface of the earth.

Following from this, the main input that is needed for the calculations of colour parameters and efficiency loss is the reflectance spectra of the samples. This also includes the angular dependence of these reflectance spectra, which is particularly significant for interference coatings. Such reflectance spectra, and their angular dependence, can be obtained by fabrication and measurements of physical samples, or alternatively, by numerical simulations.

The applied approach for calculation of colour parameters and efficiency loss is described in more detail in section 2.1. The method used for designing interference coatings and obtaining reflectance spectra by numerical simulations is discussed in section 2.2. Finally, the physical fabrication of nine samples with different coating designs, as well as their measured reflectance spectra is reported in section 2.3.

2.1. Calculation of colour parameters and efficiency loss

The approach described below for calculation of colour parameters and efficiency loss follows closely that of Røyset et al., [3]. The only new parameter introduced in this paper is the colour difference (ΔE), to be used in the analysis of angular dependent colour variation.

For colour calculations the CIE XYZ, L*a*b* and L*C*h° colour spaces [22,23] have been used. The XYZ tristimulus values are given by

$$\boldsymbol{X} = K\int_{380}^{780} \boldsymbol{R}(\lambda)\,\boldsymbol{S}(\lambda)\,\bar{\boldsymbol{x}}(\lambda)\,d\boldsymbol{\lambda} \tag{1}$$

$$\boldsymbol{Y} = K\int_{380}^{780} \boldsymbol{R}(\lambda)\,\boldsymbol{S}(\lambda)\,\bar{\boldsymbol{y}}(\lambda)\,d\boldsymbol{\lambda} \tag{2}$$

$$\boldsymbol{Z} = K\int_{380}^{780} \boldsymbol{R}(\lambda)\,\boldsymbol{S}(\lambda)\,\bar{\boldsymbol{z}}(\lambda)\,d\boldsymbol{\lambda} \tag{3}$$

$$\boldsymbol{K} = \frac{1}{\int_{380}^{780} \boldsymbol{S}(\lambda)\,\bar{\boldsymbol{y}}(\lambda)\,d\boldsymbol{\lambda}} \tag{4}$$

where $\bar{x}(\lambda)$, $\bar{y}(\lambda)$ and $\bar{z}(\lambda)$ are the colour matching functions, R(λ) is the reflectance, S(λ) is the illuminant spectrum in units of W/m^3. We have used CIE 1931 2° observer for the colour matching functions, and D65 as illuminant. The D65 is defined by CIE and is intended to represent daylight illumination. The colour matching functions are displayed in

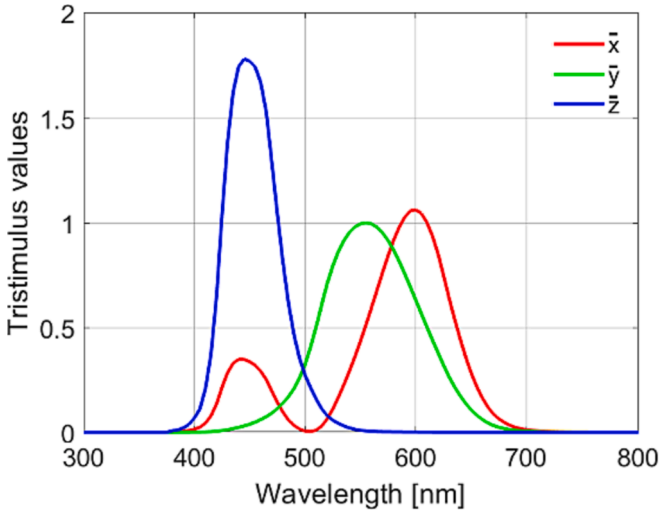

Fig. 1. The tristimulus values of the colour matching functions used in the calculations.

Fig. 1. The colour matching function $\bar{y}(\lambda)$ equals the photopic luminosity function (eye sensitivity), and Y therefore also represents the luminous reflectance.

We have also used the CIE 1976 L*a*b* colour space, which is a three dimensional, approximately uniform colour space produced by plotting L*, a*, b* in a rectangular coordinate system. The coordinates L*, a*, b* are given by

$$L^* = 116 f\left(\frac{Y}{Y_N}\right) - 16 \tag{5}$$

$$a^* = 500\left(f\left(\frac{Y}{Y_N}\right) - f\left(\frac{X}{X_N}\right)\right) \tag{6}$$

$$b^* = 200\left(f\left(\frac{Y}{Y_N}\right) - f\left(\frac{Z}{Z_N}\right)\right) \tag{7}$$

where

$$f(t) = \begin{cases} t^{\frac{1}{3}} & \text{if } t > \left(\frac{6}{29}\right)^3 \\ \frac{1}{3}\left(\frac{29}{6}\right)^2 t + \frac{4}{29} & \text{if } t < \left(\frac{6}{29}\right)^3 \end{cases} \tag{8}$$

The cube root relation holds for $L > 8$, $Y > 0.0089$ which is practically the case for all PV modules. The normalisation factors in the case of D65 illumination are $X_N = 0.95047$, $Y_N = 1.00$, and $Z_N = 1.08883$.

The L*a*b* colour space can also be expressed in terms of chroma C and hue h° by

$$C^* = \sqrt{a^{*2} + b^{*2}} \tag{9}$$

$$h^\circ = \arctan\left(\frac{b^*}{a^*}\right) \tag{10}$$

The CIE L*a*b* colour space is designed to be perceptually uniform, unlike the RGB and CMYK colour space. The L*, C*, h° closely matches human perception of lightness, chroma, and hue. Equal step changes in lightness L* represents equal step changes in perceived lightness and may therefore be most useful for displaying the impact of lightness on efficiency loss.

The colour difference [23] between reflectance angle 1 and 2 can be calculated as the root squared distance of two colours in the L*a*b* space as

$$\Delta E = \sqrt{(L_1^* - L_2^*)^2 + (a_1^* - a_2^*)^2 + (b_1^* - b_2^*)^2} \tag{11}$$

This CIE 1976 ΔE formula has been succeeded by a more perceptually uniform definition ΔE_{2000}, with formulas given in [24]. The colour parameters L*a*b* are calculated from 0° to 60°, in steps of 10°. We have introduced ΔE_{max} as a quantification of the angular dependency of a given coating design. ΔE_{max} was calculated as the maximum colour difference ΔE_{2000} between a colour in the 10°-60° range relative to normal incidence.

Colour patches were generated by transforming the X, Y, Z values to sRGB values that are plotted in Matlab.

The power conversion efficiency was modelled to be proportional to the short-circuit photocurrent density J_{sc} given by:

$$J_{sc} = \int_{300}^{1100} \frac{q\lambda}{hc} T(\lambda) I(\lambda) IQE(\lambda)\, d\lambda \tag{12}$$

where I(λ) is the AM1.5G standard solar irradiance spectrum in units of W/m^3, IQE(λ) is the internal quantum efficiency, q is the electron charge in units of C, hc/λ is the photon energy in units of J. T(λ) is the transmittance of the simulated structures, including front glass, interference layers and encapsulation. The model we have used for the IQE displayed in Fig. 2(a) is intended to represent an idealised crystalline silicon solar cell. The spectral dependence of $J_{sc}(\lambda)$ in the case T = 1 is given in Fig. 2 (b).

We have introduced a relative power conversion efficiency η_{rel} and relative loss P given by

$$\eta_{rel} = 1 - P = \frac{J_{sc}}{J_{sc,ref}} \tag{13}$$

where $J_{sc,ref}$ is the photocurrent density for a reference module with no interference layers. We can write the relative loss as:

$$P = \frac{\int_{300}^{1100} \lambda(T_{ref}(\lambda) - T(\lambda)) I(\lambda) IQE(\lambda) d\lambda}{\int_{300}^{1100} \lambda T_{ref} I(\lambda) IQE(\lambda) d\lambda} \tag{14}$$

where T and T_{ref} are the transmittance with and without interference coating.

This model for relative power conversion efficiency assumes that the reduction in J_{sc} is the dominating contribution to efficiency reduction and that the variation in diode open-circuit voltage and fill factor can be neglected. A more detailed diode model has been used in [4] for the study of colour dependent efficiency. From these results on colour dependent open-circuit voltage and fill factor we have concluded that the variation in Jsc is much larger than the variation in open-circuit voltage and fill factor.

For the discussion of different contributions to loss we have defined the contributions to the relative loss P as

$$P = P_{UV} + P_{VIS} + P_{NIR} \tag{15}$$

where P_{UV}, P_{VIS}, and P_{NIR} are the relative loss contributions from the

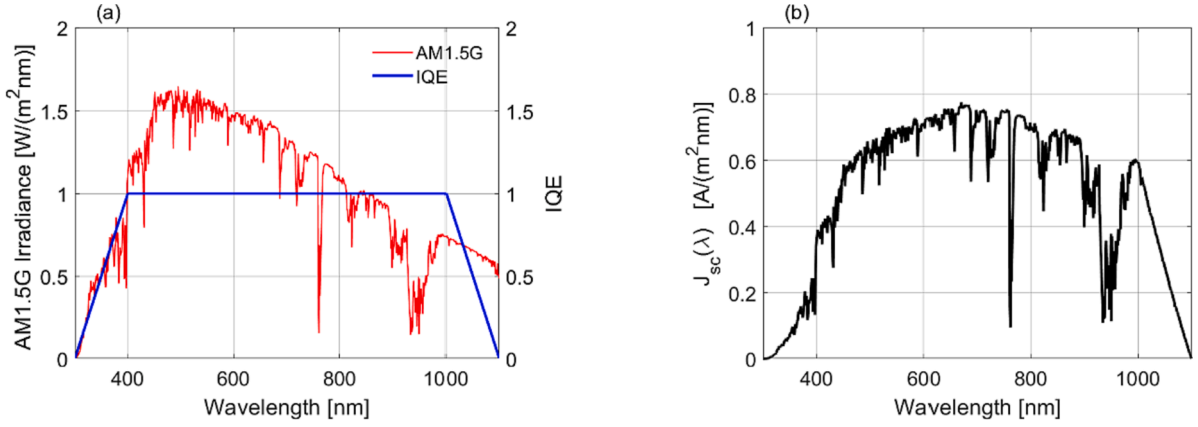

Fig. 2. (a) Solar irradiance spectrum and internal quantum efficiency used in the calculations. (b) The resulting photocurrent density $J_{sc}(\lambda)$ spectral dependence in the case T = 1.

ultraviolet (UV) (300–400 nm), visible (VIS) (400–700 nm) and near infrared (NIR) (700–1100 nm) wavelength regions, respectively.

In Røyset et al., a colour performance index, CPI, was introduced, which quantifies the relation between the luminous reflectance Y and the relative loss P:

$$CPI = \frac{Y}{P} \tag{16}$$

This definition of CPI allows for comparison of colours with different lightness. Considering a case with the same spectral reflectance across all wavelengths (grey), CPI will equal 1, independent of the magnitude of reflectance. By increasing the reflectance in the visible wavelength region and reducing the reflectance in the NIR wavelength region, the CPI becomes>1. A high CPI can be obtained by having a high reflectance where the eye sensitivity $\bar{y}(\lambda)$ is largest, and a low (or zero) reflectance outside this spectral range.

2.2. Coating design and numerical simulations

The spectral reflectance characteristics of optical interference coatings depend on several design parameters, such as the number of layers, design wavelength, layer thicknesses, and refractive indices of the layers.

The choice of the layer structure for a coating design will therefore affect the efficiency as well as the visual properties of the PV module, including the angular colour dependence. The interaction between coating design parameters, the visual properties and the efficiency is shown in Fig. 3, illustrating that the design parameters affect the visual properties and efficiency, but also the interdependence of visual properties and efficiency.

The basic film structure of an interference coating is that of a reflectance filter [25], where the reflected photons from each interface interferes constructively at a given design wavelength λ_D. The layers are high (H) or low (L) index layers with refractive indices n_H and n_L respectively, with thicknesses $L_H = M\lambda_D/4n_H$ and $L_L = M\lambda_D/4n_L$. M is an integer and is the thickness normalised to a quarter-wavelength layer. For M = 1, the thickness is equal to one quarter wave layer, for M = 2, the thickness is equal to 2 quarter wave layers, etc. M is therefore defined as the layer thickness parameter which determines whether the interference peak is the first order (M = 1), second order (M = 3) or third order (M = 5). Simultaneously, destructive interference minima appear for M = 2, 4, and 6, which means that a constructive interference peak at λ_D has neighbouring reflection minima at $\lambda_D M/(M-1)$ and $\lambda_D M/(M+1)$. Increasing M will therefore reduce the width of the interference peak and the distance between neighbouring peaks.

Note that the resulting colour generated by the reflectance filter depends on all of the coating design parameters, and not only the design wavelength λ_D. Therefore, a choice of a given design wavelength does not necessarily imply a desire to obtain a hue that matches the given wavelength.

The number of layers parameter N can have odd values N = 1, 3, 5, etc., resulting in an even number of interfaces which is practical for the design of low reflectance between neighbouring peaks. Increasing the number of layers increases the peak reflectance since a larger number of interfaces contributes to the constructive interference. Increasing the number of layers N decreases the width of the interference peak and increases the width of the low reflectance range between the peaks.

Fig. 4(a) illustrates a typical case of a N = 5 (HLHLH) reflectance filter where n_s equals the refractive index of the surrounding medium. Fig. 4(b) illustrates an N = 5 case with higher film refractive indices. Between the interference peaks a very low reflectance is desirable. This can be obtained by having the same index contrast n_L/n_H at all interfaces. The design in Fig. 4(b) therefore has two additional n_a layers in order to achieve this. The optimum n_a refractive index is given by $n_H/n_a = n_a/n_0$. The two additional layers are not needed to achieve high reflectance at the interference peaks, only to keep the reflectance low between them, which is particularly important for the NIR wavelength region. In a case where the interference layers are positioned at the backside of the front glass, the surrounding medium will be glass and EVA with a refractive index n_s close to 1.5.

In addition to the number of layers N, and layer thickness parameter M, the refractive index contrast plays an important role since the reflectance at each interface is $(n_H\text{-}n_L)^2/(n_H + n_L)^2$ in the case of normal incidence. In addition to influencing the reflectance, the refractive index also affects the angular dependence. For non-normal (oblique) angle of incidence, the wavelength that corresponds to constructive interference in a film layer, shifts from λ_D to $\lambda_D \cos(\theta_F)$ where θ_F is the angle in the film layer with index n, given by Snell's equation $n^*\sin(\theta_F) = \sin(\theta_O)$ where θ_O is the incidence angle in air. Hence increasing n reduces θ_F and thereby reduces the angular dependence. The angular dependence can be reduced by either increasing n_H or n_L or both.

For a more comprehensive investigation of the coating design parameters, a matrix with N = 1, 3, and 5, M = 1, 3, and 5, λ_D = 450, 550, and 650 nm was simulated using Essential MacLeod (version 11), a software made for design and analysis of thin film optical coatings based on the transfer matrix method. The simulated layer structure for the case of N = 3, M = 3, λ_D = 550 nm is illustrated in Fig. 5(a) and (b) for the low index case (n_H/n_L = 2.0/1.5) and the high index case (n_H/n_L = 2.3/1.8),

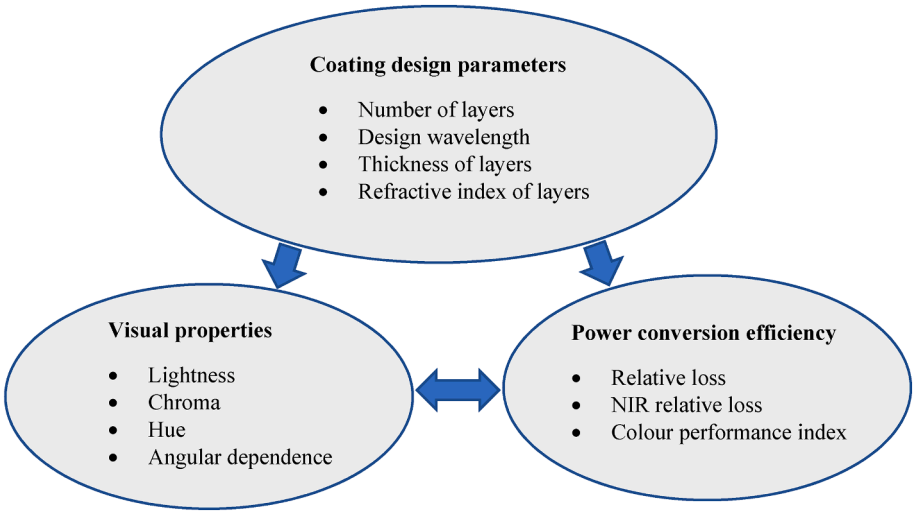

Fig. 3. The interdependence of visual properties and efficiency, and their dependence on coating design parameters.

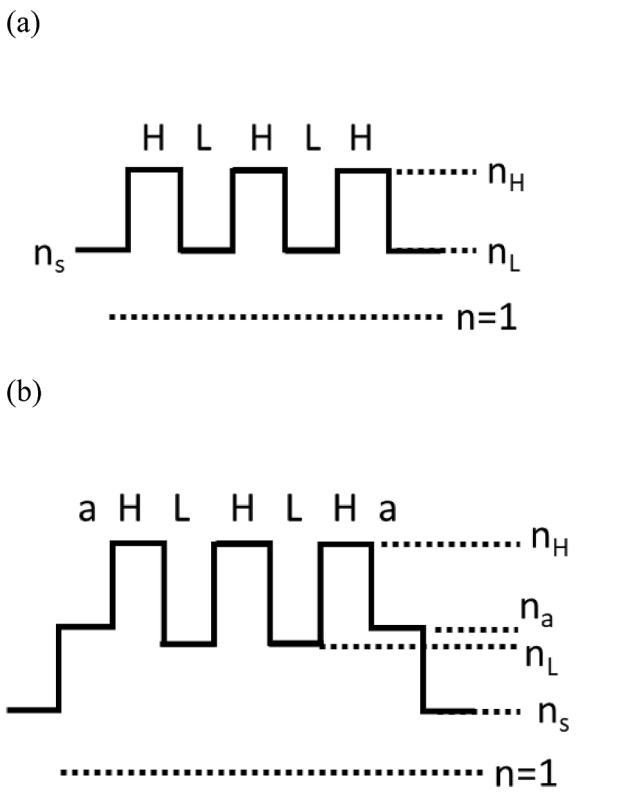

Fig. 4. Illustration of the refractive index profile of a N = 5, five-layer HLHLH reflectance filter. Low refractive index case (a) where n_L matches the surrounding medium n_s, and high refractive index case (b) where both n_H and n_L is higher than the refractive index n_s of the surrounding medium. In this case additional layers, a, may be added to improve the reflectance profile.

respectively. The short notation N3M3 corresponds to N = 3, M = 3.

In our simulation model all interfaces are parallel, and surface roughness is not included in the model, implying that the observation angle equals the angle of incidence θ_O. The absence of surface roughness has some important practical implications with respect to the visual observation of colour. In direct sunlight, when looking at the mirror image of the sun, the high luminance of the sun will completely dominate any sensation of colour, making visual colour observation impossible. On a clear day it is still possible to see the colours, provided that the observer does not look in the direction of the mirror image of the sun. In this case the light source will in practice typically be the blue sky, which is slightly different from the D65 illuminant that is used in our simulation model. Therefore, the colours resulting from our simulations most realistically represent the colours that can be observed on a fully overcast day. The spectral composition of the overcast sky is very similar to the D65 illuminant.

Bläsi et al., [18] have demonstrated that high refractive indices combined with a surface roughness for the front glass can be exploited to reduce the angular dependence of the colour.

The additional low index layers have M = 4, not M = 3. Because the additional layer a has one interface to a lower refractive index and one interface to a higher refractive index, as opposed to the H and L layers, this additional layer must have even M to obtain constructive interference. Thus, for reducing unwanted reflection peaks, i.e., suppressing side oscillations, the thickness of the additional layers in the optical interference coating for the high index case was set to M = 4 in this study, but it is also possible to use for example M = 2 to reduce the total thickness of the stack [18].

The simulated reflectance R(λ) and transmittance T(λ) spectra are transferred to Matlab for calculation of colour parameters and relative power conversion efficiency.

(a)

Air				
Porous SiO2		n=1.23	L=132nm	
Glass		n=1.52		
SiNx	H	n_H=2.05	L=201nm	M=3
SiO2	L	n_L=1.46	L=289nm	M=3
SiNx	H	n_H=2.05	L=201nm	M=3
EVA		n=1.49		

(b)

Air				
Porous SiO2		n=1.23	L=132nm	
Glass		n=1.52		
Y2O3	a	n_a=1.79	L=307nm	M=4
TiO2	H	n_H=2.32	L=178nm	M=3
Y2O3	L	n_L=1.79	L=231nm	M=3
TiO2	H	n_H=2.32	L=178nm	M=3
Y2O3	a	n_a=1.79	L=307nm	M=4
EVA		n=1.49		

Fig. 5. Illustration of the simulated thin film layer structure in the MacLeod software in the case of N = 3, M = 3 (N3M3) and λ_D = 550 nm. Corresponding thickness of the layers and refractive indices at 550 nm are also given. Structure (a) is the low index case (n_H/n_L = 2.0/1.5) while the high index case (n_H/n_L = 2.3/1.8) is given in (b).

2.3. Experimental fabrication and characterisation

To demonstrate the effect of the layer number parameter N and the layer thickness parameter M, a matrix of nine different laminated samples were fabricated, with coating designs consisting of N = 1, 3, 5 and M = 1, 3, 5, with λ_D = 630 nm, n_L = 1.5, and n_H = 2.0. The fabricated sample case of N = 5 (HLHLH) is illustrated in Fig. 6, where the interference layers are inserted between the glass and ethylene–vinyl acetate (EVA) laminate on the front side of the silicon wafer.

The samples were prepared using (1 0 0)-oriented, p-type CZ monocrystalline silicon wafers with a thickness of 200 μm as substrates. The wafers were surface textured by etching in 30 % KOH at 75 °C for 2 min and subsequent cleaned in 20 % HCl at room temperature for 5 min and rinsed in deionized water. An 80 nm thick anti-reflection coating (ARC) of hydrogenated amorphous silicon nitride (a-SiN_x:H) was deposited onto the silicon substrate at 350 °C using an Oxford Instruments PlasmaLab System133 PECVD tool with a gas mix of silane, ammonia, and nitrogen.

Interference coatings with a design wavelength λ_D = 630 nm were prepared by depositing hydrogenated amorphous silicon oxide (a-SiO_x:H), with a gas mix of silane, nitrous oxide, and nitrogen, and a-SiN_x:H at 350 °C onto a microscope slide glass (Thermo scientific Menzel-Gläsers) of 1 mm thickness. Interference coatings were fabricated with various thin film thicknesses and number of layers according to Table 1. The glass with interference coating on the rear side was subsequently

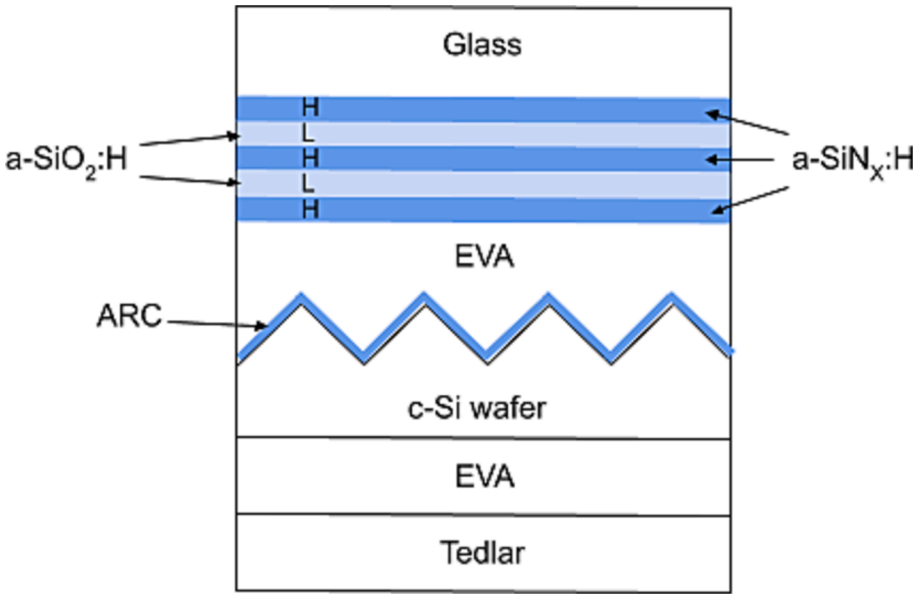

Fig. 6. Schematic overview of the experimental sample design for the case of N = 5 (HLHLH).

Table 1
Individual and total film thickness for nine fabricated samples of different coatings designs, all with a design wavelength $\lambda_D = 630$ nm. A reference sample (N0M0) with no thin film layers was also included.

Sample ID	N	M	Film thickness [nm]					Total thickness (nm)
			a-SiN_x:H	a-SiO_x:H	a-SiN_x:H	a-SiO_x:H	a-SiN_x:H	
N1M1	1	1	78	–	–	–	–	78
N3M1	3	1	78	105	78	–	–	261
N5M1	5	1	78	105	78	105	78	444
N1M3	1	3	234	–	–	–	–	234
N3M3	3	3	234	315	234	–	–	783
N5M3	5	3	234	315	234	315	234	1332
N1M5	1	5	390	–	–	–	–	390
N3M5	3	5	390	525	390	–	–	1305
N5M5	5	5	390	525	390	525	390	2220
N0M0	0	0	–	–	–	–	–	0

laminated to the silicon substrate using a tedlar backsheet and EVA at 150 °C in a P.Energy L036A laminator. In addition to nine samples with different N and M, a glass with no thin film layers (N = 0, M = 0) was laminated to a silicon substrate, serving as a reference sample. Note that metal contacts were omitted from front and rear side of the silicon wafers to simplify the optical reflectance measurements and corresponding analysis.

The refractive index (n), extinction coefficient (k), and thickness of the a-SiN_x:H and a-SiO_x:H thin film layers were determined using a variable angle spectroscopic ellipsometer (Woollam VASE). The measured ellipsometry data was modelled using the software WVASE32 from Woollam. Optical reflectance spectra were measured for the nine laminated samples and the results were used to compare and verify the spectra obtained by numerical modelling using the MacLeod software. The angle-dependent optical reflectance was measured with monochromatic light for wavelengths ranging from 350 nm to 1100 nm using a home-built spectral response measurement system consisting of a Newport Oriel Apex illuminator with a Cornerstone 260 monochromator, a set of collimating and focusing lenses, and a 150 mm integrating sphere (Labsphere model RTC-060-SF) with a centre-mounted sample holder which can be rotated to the desired angle of incidence. A quartz crystal achromatic depolarizer (Thorlabs model DPU-25) was used in the beam path to randomize the partly polarized light from the monochromator. A silicon photodiode detector (Hamamatsu model S1336-5BQ) mounted at the bottom of the integrating sphere was used to collect the reflected beam from the sample. The angle of incidence for the reflectance measurements was varied from 10° to 70°, in steps of 10°.

3. Results

In this section we present the main results from our work. Results from measurements on the fabricated samples are presented in section 3.1. Numerical simulation results related to colour and angular colour dependence are presented in section 3.2. and 3.3 respectively. Numerical simulation results regarding efficiency are discussed in section 3.4. Finally, a short summary of the most important findings in the form of design guidelines is provided in section 3.5.

3.1. Experimental results

The fabricated structures were investigated and compared with numerical simulations, i.e., the optical reflectance spectra for modelled structures were computed using the MacLeod software with film thicknesses and refractive indices similar to that for the fabricated structures. The refractive indices and extinction coefficients determined from ellipsometry are displayed in Table 2 along with refractive indices from the MacLeod simulations. The extinction coefficient for the SiN_x layer is considered sufficiently low to not have a significant impact on the design of the optical interference coatings.

Table 2
Refractive indices and extinction coefficients measured with spectroscopic ellipsometry compared with those used in the numerical simulations.

		SiO_2		SiN_x	
	Wavelength	n	k	n	k
Experimental	550 nm	1.502	0	2.039	0.0002
	630 nm	1.499	0	2.022	0.00007
Simulation	550 nm	1.504	0	2.050	0.0002
	630 nm	1.500	0	2.039	0.0001

Fig. 7(a) shows a photograph of the nine different samples, each sample 26 mm × 38 mm in size, that were fabricated and analysed in this work. The picture was taken at an angle of approximately 10°, using a 12-megapixel camera with an F/1.8 aperture lens with 27 mm equivalent focal length. The light source in this case was overcast daylight at noon, corresponding to the CIE D65 illuminant.

The measured reflectance spectra for the nine coloured samples and the reference sample (N0M0) are displayed in Fig. 8(a)-(c), along with the corresponding simulated reflectance spectra, using a design wavelength of 630 nm in the simulation model. The graphs show that there is a good correspondence between the measured and simulated reflectance spectra, suggesting that the numerical model can be used to accurately predict the optical response of experimental samples. The minor deviations can be ascribed to slight discrepancies in the layer thickness and refractive index. Also, the bottom four layers in the experimental structure in Fig. 6 (ARC, c-Si, EVA, and Tedlar) are not included in the simulation model, cf. Fig. 5. This causes a discrepancy between measured and simulated reflection for $\lambda > 1000$ nm, where the experimental reflectance is higher compared to that of the modelled reflectance due to infrared light being transmitted through the laminated c-Si sample during measurement. The transmitted light is then reflected to the detector, resulting in an increase in the measured signal. This does, however, not contribute to the calculated colours as it is outside the visible wavelength range and gives only minor deviation to the efficiency calculations as the IQE of the solar cell is low in this spectral region.

The CIE L*a*b* parameters for the experimental samples were calculated based on the measured reflectance spectra at 10° incidence angle and are summarized in Table 3 along with the chroma parameter c*. The corresponding colour patches are shown in Fig. 7(b). Both from the colour patches and the results in Table 3, we observe a large variation in lightness, chroma, and hue for the experimental samples.

The measured reflectance spectra for an incidence angle of 10°, 30°, 50° and 70° for N3M3 are displayed in Fig. 9(a). As the angle of incidence increases, the colour changes from red to green. At 70° a strong baseline reflectance at the glass front surface contributes to a large reduction in chroma and an increase in lightness. The angle dependent colour patches were calculated from the measured spectra and are displayed in Fig. 9(b), whereas the corresponding simulated spectra are shown in Fig. 9(c). In all cases there is a strong variation in chroma, hue and lightness. The agreement between colour patches calculated from experimental and simulated spectra is good.

3.2. Numerical results on colour

For a more detailed study of the effect of N, M and the design wavelength λ_D on the visual properties and the efficiency of the PV module, we simulated the variation of N = 1, 3, 5 and M = 1, 3, 5 for design wavelengths of 450 nm, 550 nm and 650 nm, and refractive indices (2.0/1.5). The 550 nm case was also simulated for a set of higher refractive indices (2.3/1.8). The simulated structures are illustrated in Fig. 5 for the 550 nm case. The simulation parameters and corresponding results for colour, efficiency and angular dependence are given in Table 4 for these 36 cases. In the table we have only given the relative loss in the NIR region, not in the UV or VIS region. Due to the solar

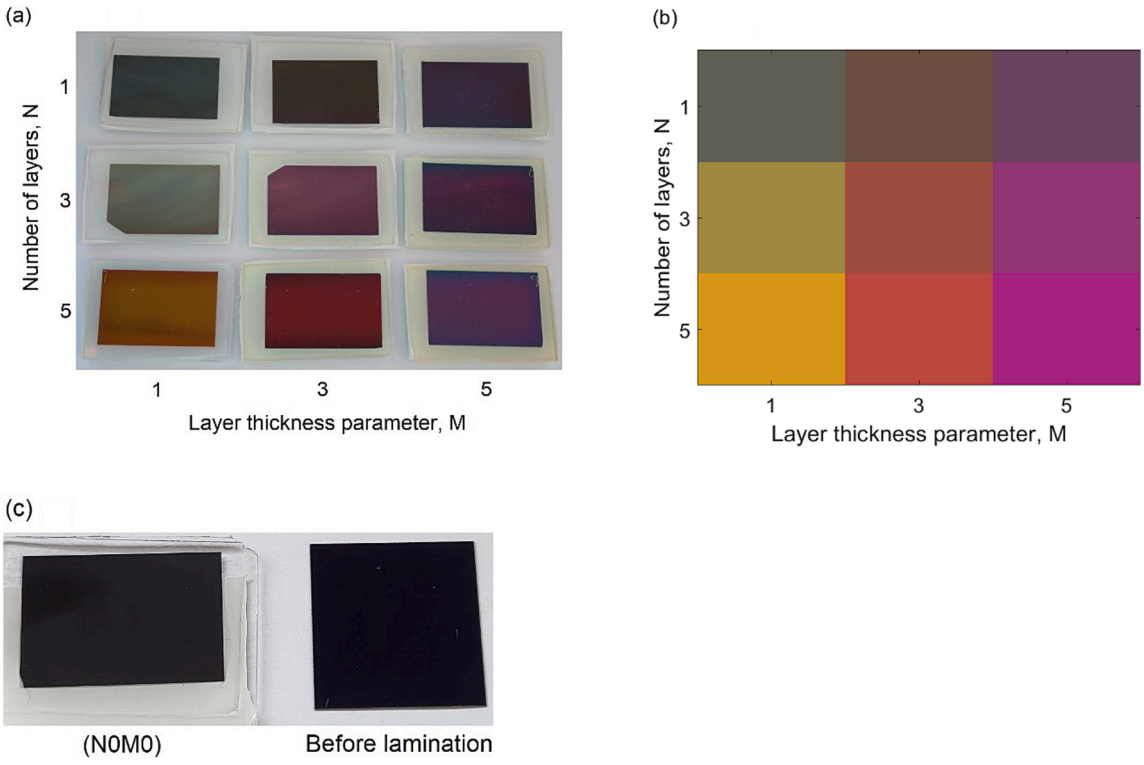

Fig. 7. (a) Photograph of the nine 26 mm × 38 mm fabricated samples and (b) corresponding colour patches computed from simulated spectra, with the number of layers N and layer thickness parameter M indicated for each sample, and with a design wavelength $\lambda_D = 630$ nm. (c) Photograph of the reference sample (N0M0) along with the prepared c-Si sample before lamination, The photographs were taken at an angle of approximately 10° from normal incidence in overcast daylight at noon.

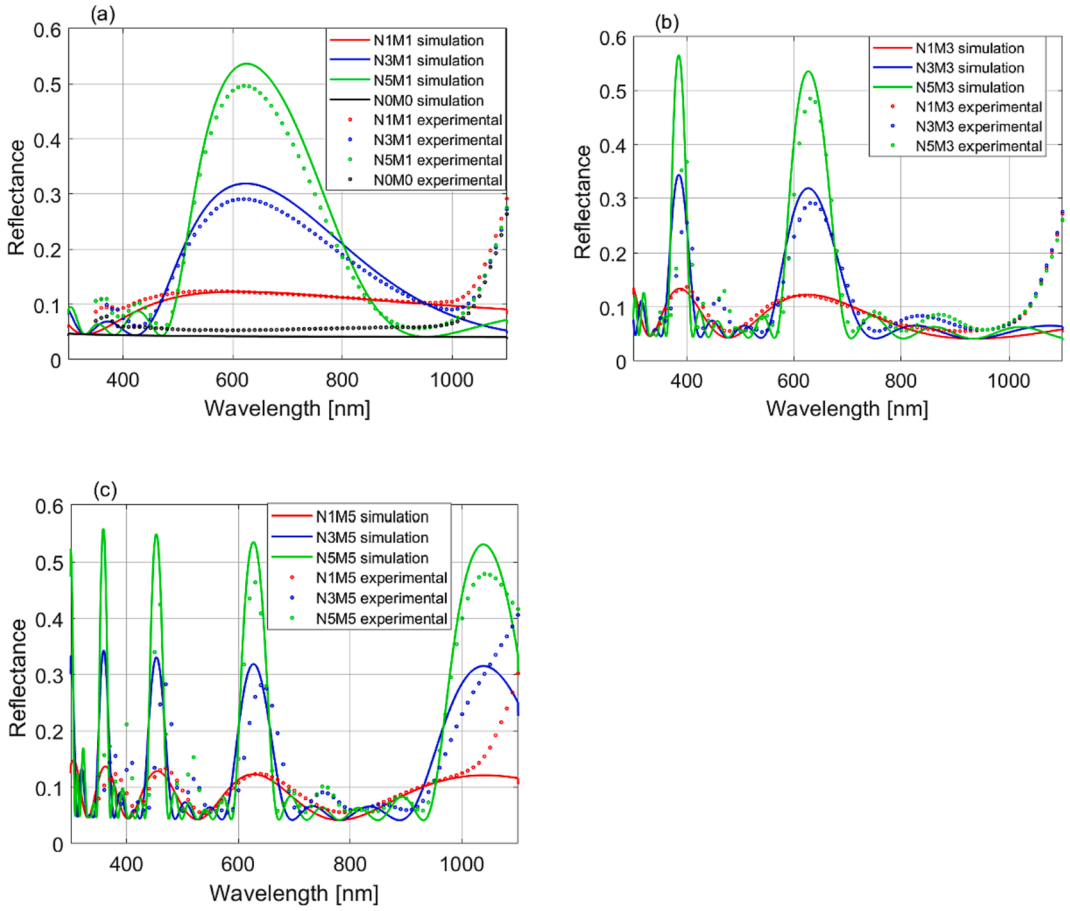

Fig. 8. Experimental (dotted) and simulated (solid) reflectance spectra for different number of layers for (a) M = 1, (b) M = 3, and (c) M = 5. Also shown in (a) are the reflectance spectra for the reference sample (N0M0). The angle of incidence is 10° for both experimental and simulated spectra.

Table 3
Colour parameters computed from measured reflectance spectra.

Sample ID	N	M	L*	a*	b*	c*	h°	sRGB colour patch
N1M1	1	1	41.7	-1.4	2.9	3.2	115.7	
N3M1	3	1	56.6	-2.0	35.2	35.3	93.3	
N5M1	5	1	66.4	8.3	54.1	54.7	81.3	
N1M3	1	3	37.6	6.5	8.1	10.4	51.5	
N3M3	3	3	40.6	33.3	7.4	34.1	12.5	
N5M3	5	3	43.8	44.1	12.4	45.8	15.7	
N1M5	1	5	34.4	14.1	-8.5	16.4	329.0	
N3M5	3	5	37.2	22.6	-14.9	27.1	326.6	
N5M5	5	5	41.7	38.8	-17.4	42.5	335.9	
N0M0	0	0	27.7	0.6	-1.7	1.8	289.7	

irradiance spectrum, as well as the internal quantum efficiency of the silicon cell, the relative losses in NIR are much more important than in UV, as can be seen from Fig. 2. Losses in the VIS region are in another category compared to UV and NIR, since losses in VIS are required to create the colours. The results given in Table 4 are for normal incidence, The ΔE_{max} is the maximum colour difference between the colour with normal incidence and a colour in the 10°-60° range.

The simulated spectra of the 550 nm, low index (2.0/1.5) cases are shown in Fig. 10(a)-(c), along with the corresponding computed colour patches in Fig. 10(d). An important spectral feature is that as M increases

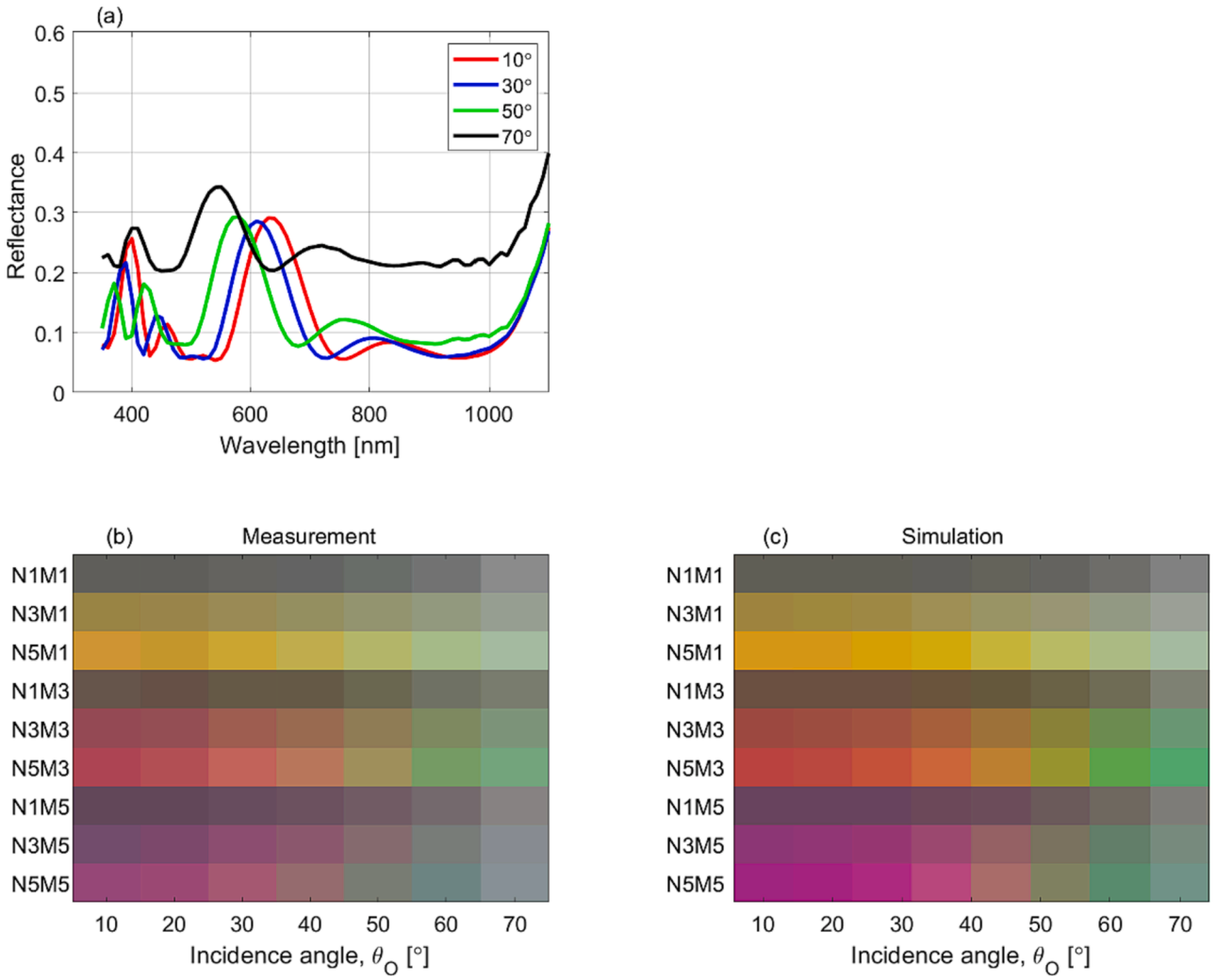

Fig. 9. Measured reflectance spectra from experimental samples for N = 3, M = 3 at incidence angles of 10°, 30°, 50° and 70° (a). Angle dependent colour patches calculated from experimental spectra (b) and simulated spectra (c).

from 1 to 3, the width of the 550 nm interference peak decreases, leading to higher chroma. For M = 3, the width is quite narrow, and a further narrowing with M = 5 only results in a slight increase in chroma. An increase in N, from 1 to 3, for a given M, leads to a higher amplitude of the interference peak, and a large increase in lightness. But for a further increase of N from 3 to 5, a much smaller increase in lightness is observed due to narrowing of the peak width. On the other hand, an increase in N gives a significant increase in chroma, in all three cases of M = 1, 3 and 5.

Some of the same features of lightness and chroma can be observed also for design wavelengths of 450 and 650 nm, which are displayed in Fig. 11. For all design wavelengths, an increase in N leads to a significant increase in chroma. The main difference between the 550 and the 450/650 cases is that 550 nm is centred on the peak of the eye sensitivity, and there is only one peak within the visible range 400–700 nm. For a peak wavelength of 450 or 650 nm, a change in amplitude and width will also result in a significant change in hue. This effect is largest for the 650 nm case, which for M = 1 has a large tail into green, resulting in an orange colour, and for M = 5, where the neighbouring peak at about 480 nm results in a purple colour. For both 450 and 650 nm the lightness is reduced as M increases due to a reduced tail into the part of the spectrum with highest eye sensitivity.

The combined effect of N and M on lightness and chroma is displayed in Fig. 12. The lines connect the results for the same λ_D and M, and in all cases, N = 5 results in the highest chroma. From Fig. 12 and Fig. 11(d) and (h), we also observe that for 450 and 650 nm and M = 3, 5 quite dark colours are obtained due to narrow reflection peaks outside the highest eye sensitivity range. These results show that by varying N, M and λ_D, a large variation in lightness, hue and chroma can be obtained.

3.3. Numerical results on angular dependence

Another feature of interference coatings that needs attention is the angular dependence of the observed colours. Fig. 13 shows that the interference peak shifts to shorter wavelengths with increasing incidence angle θ_O. The same blueshift of the interference peak is observed in the experimental results in Fig. 9(a). We observe that the measured reflectance spectra shown in Fig. 9(a) have a larger front glass reflectance than the simulation results shown in Fig. 13. The difference is due to the absence of an anti-reflection coating for the experimental samples, causing larger front glass reflectance at all incidence angles. There is an increased baseline reflectance for large incidence angles, mainly due to increased reflectance from the first surface of the front glass. The change of colour with observation angle is a feature that can be utilized by architects to create an aesthetic effect, as was demonstrated several years ago on the façade of Copenhagen International School. Here the PV modules were slightly tilted with respect to each other in order to create a distinct visual effect. In many other cases, however, an angular dependent colour may be considered as a significant drawback from an aesthetic viewpoint.

Table 4
Simulation results for different coating design parameters.

Refrac-tive index	Design wave-length	Number of layers parameter	Layer thickness parameter	Light-ness	Chroma	Hue	Maximum colour difference	Relative loss	NIR relative loss	Colour perfor-mance index	sRGB colour patch
n_H/n_L	λ_D	N	M	L*	c*	h°	ΔE_{max}	P	P_{NIR}	CPI	
	[nm]					[°]		[%]	[%]		
2.0/1.5	450	1	1	34.4	4.8	261.2	5.0	6.45	2.69	1.15	
		3	1	54.8	18.4	240.9	10.2	11.33	1.03	1.90	
		5	1	61.2	38.8	236.5	29.3	15.14	1.85	1.87	
		1	3	22.4	24.9	253.9	15.6	3.89	2.26	0.79	
		3	3	21.2	79.8	303.2	13.4	5.66	2.20	0.52	
		5	3	23.0	106.4	307.4	23.2	6.37	1.68	0.54	
		1	5	14.7	46.2	311.7	20.9	4.90	2.88	0.33	
		3	5	16.3	87.2	311.4	32.2	9.72	6.20	0.21	
		5	5	17.4	108.4	313.0	35.0	13.07	8.87	0.17	
	550	1	1	36.4	2.5	261.2	3.4	7.24	3.13	1.17	
		3	1	62.7	17.4	240.9	16.1	16.53	3.97	1.82	
		5	1	78.0	40.2	236.5	30.8	21.73	2.34	2.39	
		1	3	34.7	20.0	253.9	9.9	3.46	0.60	2.01	
		3	3	55.0	65.5	303.2	51.1	6.18	0.63	3.36	
		5	3	64.8	87.5	307.4	64.2	8.21	0.58	3.82	
		1	5	32.1	21.7	311.7	9.9	5.11	2.96	1.23	
		3	5	47.6	58.4	311.4	36.9	10.77	6.53	1.45	
		5	5	55.1	74.2	313.0	47.2	14.28	8.59	1.54	
	650	1	1	36.9	3.4	124.7	2.6	7.64	3.55	1.15	
		3	1	56.5	45.4	87.7	15.7	19.27	8.83	1.23	
		5	1	64.6	61.9	70.8	27.0	26.00	10.19	1.27	
		1	3	28.9	18.2	348.2	29.8	4.34	1.09	1.16	
		3	3	33.6	44.3	6.8	55.1	8.40	1.22	0.86	
		5	3	35.9	54.4	9.3	66.9	11.24	0.96	0.75	
		1	5	25.6	26.9	315.5	10.7	4.78	1.60	0.84	
		3	5	29.8	49.9	320.9	41.2	9.36	2.83	0.61	
		5	5	32.2	60.5	321.2	54.0	12.32	3.61	0.55	
2.3/1.8	550	1	1	45.3	28.7	127.6	18.9	5.28	0.35	2.49	
		3	1	62.3	49.5	122.7	25.3	10.18	0.53	2.85	
		5	1	73.4	71.3	119.6	29.3	13.29	0.09	3.29	
		1	3	38.7	49.1	131.6	19.7	3.43	0.71	2.54	
		3	3	50.1	74.0	130.7	24.8	5.47	0.99	3.02	
		5	3	56.6	87.5	131.0	27.7	6.49	0.71	3.43	
		1	5	33.2	28.6	159.3	8.6	5.24	2.78	1.29	
		3	5	42.0	45.2	150.6	16.0	8.69	4.72	1.34	
		5	5	47.1	54.4	147.8	20.3	11.37	6.25	1.34	

Colour parameters for incidence angles ranging from 0° to 70° have been calculated in steps of 10°, and the corresponding colour patches are shown in Fig. 14 (a)-(d) for varying N, M and λ_D. The calculated maximum colour differences ΔE_{max} are given in Table 4.

For all λ_D, the colours with lowest angular dependence are achieved when either N or M equals 1. The structures with $N = 1$ or $M = 1$ correspond to the broadest interference peaks and lowest chroma. Broad reflectance peaks cause most of the reflectance spectrum to remain almost unaltered. Structures with $N > 1$ and $M > 1$ result in narrow interference peaks and high chroma. High chroma combined with a change in hue, due to the wavelength shift, cause a much larger change in a* or b*, hence a larger colour difference ΔE_{2000}. The colour difference due to a variation in lightness L* is much smaller than the colour difference due to a variation in hue h° or chroma c*. We should therefore expect a strong covariation between ΔE_{max} and the chroma of the colour, and a smaller covariation for ΔE_{max} and lightness. Maximum colour difference ΔE_{max} versus lightness and chroma are displayed in Fig. 15 (a) and (b), respectively. ΔE_{max} is the maximum colour difference relative to the colour with normal incidence. From Fig. 15 (b) we observe that there is a strong covariation between angular dependence and chroma.

N3M1 combines low angular dependence ($\Delta E_{max} < 20$) with high lightness ($L^* > 40$) but cannot be combined with a high chroma ($c^* > 40$), except for $\lambda_D = 650$ nm. The low angular dependence of N3M1 can also be observed from Fig. 14.

The angular colour dependence will be somewhat reduced if the refractive indices are increased. From Table 4 and Fig. 14 we observe

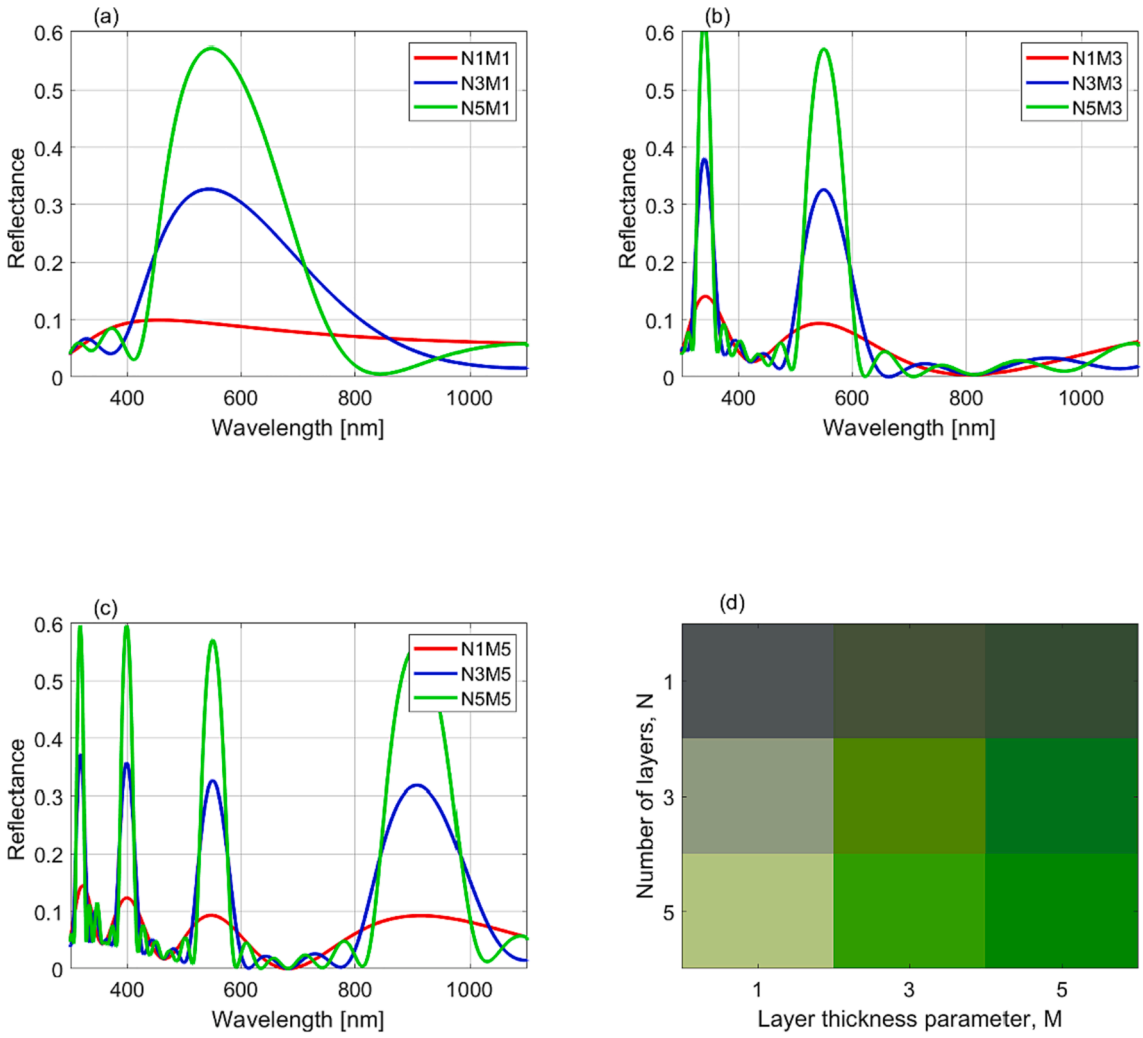

Fig. 10. Simulated reflectance spectra for a low index design (2.0/1.5) with λ_D = 550 nm and a layer thickness parameter (a) M = 1, (b) M = 3, and (c) M = 5. Corresponding colour patches are displayed in (d). All cases are for normal incidence.

that the maximum colour difference ΔE_{max} may be smaller for high refractive indices. When comparing the maximum colour difference ΔE_{max} for the low and high index designs for λ_D = 550 nm in Table 4, it is important to note that the difference in chroma may have a larger influence on the colour dependence than the difference in refractive index. By comparing the N5M3 case, which have comparable chroma, we observe that the angle dependence is significantly reduced to about 60% in the high index case. The wavelength of constructive interference is given by $\lambda = \lambda_D \cos(\theta_F)$ and $n^*\sin(\theta_F) = \sin(\theta_O)$. The interference peak wavelength versus incidence angle is displayed in Fig. 16 for the 550 nm design case. The peak wavelength is calculated as the average of the two constructive interference wavelengths given by the two indices in the film layers. An increase in the refractive index reduces the angle in the film layer, and the angular dependence is therefore reduced.

Increasing the refractive indices is therefore an effective approach to reduce the angular dependence of the colour. A disadvantage of using high refractive indices is the need for additional layers to reduce the reflectance between the interference peaks. Additional layers will add complexity and cost. Moreover, some high index materials such as TiO_2 may have higher absorption compared to that of commonly used low index materials.

3.4. Numerical results on efficiency

In addition to having a large impact on the visual appearance (colour), the coating design parameters N, M and λ_D also have a large impact on the efficiency of the PV module. The light reflected by the interference coating will not be available for current generation, and the efficiency will be reduced relative to the case with no interference coating. Design parameters N, M and λ_D affect both the visual properties and the efficiency, and there are design trade-offs between efficiency and lightness, chroma, and hue. The most obvious is the effect of lightness, because an increase in lightness leads to fewer photons being available for charge carrier generation. This covariation is displayed in Fig. 17. Increasing N always gives an increase of the relative loss P, and in most cases also results in an increased lightness. N3M3 and N5M3 with λ_D = 550 nm are the best options to achieve high efficiency and high lightness simultaneously.

The effect of increasing M is more complex. For 550 nm, M = 3 gives a good trade-off between lightness and efficiency. The reason for this is twofold: (i) M = 3 and 5 gives a narrower reflection peak than M = 1, and therefore most of the reflected light is in the wavelength range where the eye is most sensitive; (ii) However, as M is increased from 3 to 5, the distance between neighbouring reflection peaks is reduced, and the broad reflection minimum in the NIR wavelength range is replaced by a strong interference peak that can contribute strongly to reduced efficiency. If this interference peak appears between λ = 700 nm and the Si bandgap of λ = 1100 nm, the efficiency will be reduced. The NIR contribution to the relative loss is displayed in Fig. 18 and shows that M = 3 gives the lowest NIR loss. For M = 3, green colours give the lowest

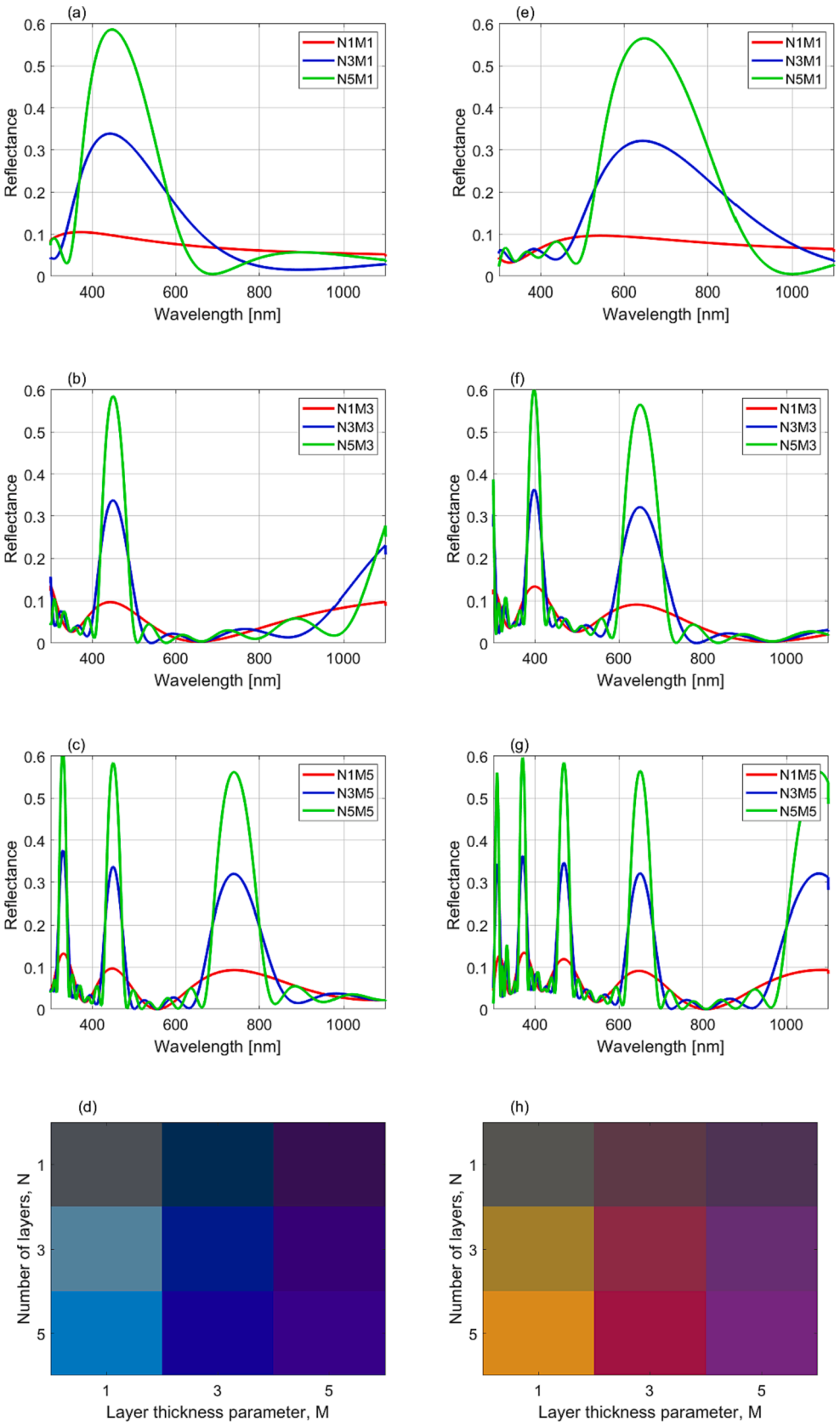

Fig. 11. Simulated reflectance spectra for a low index design (2.0/1.5) with $\lambda_D = 450$ nm (a)-(d) and 650 nm (e)-(h) for layer thickness parameter M = 1 (a and e), M = 3 (b and f), and M = 5 (c and g). Corresponding colour patches are displayed in (d) and (h). All cases are for normal incidence.

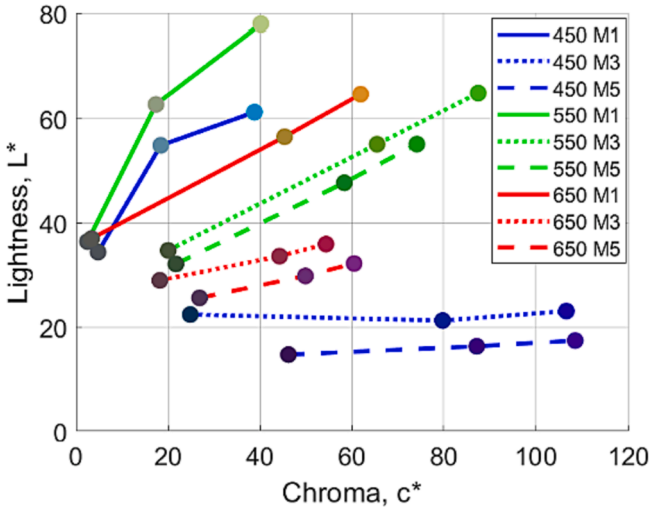

Fig. 12. Relation between lightness L* and chroma c* for different N, M and λ_D. The lines connect the results for N = 1, 3, 5 and serve as a guide to the eye. Lowest chroma is obtained for N = 1. The colour of the symbols is the same as the colour patches in Figs. 10 and 11.

NIR loss. Blue and red colours have stronger tails from an interference peak into the 700–1100 nm spectral band. Increasing M from 3 to 5 increases the NIR loss and decreases the efficiency for all colours.

For λ_D = 450 nm, high lightness can be obtained for N3M1 and N5M1 but at a higher efficiency loss. For λ_D = 650 nm, high lightness can also be obtained for N3M1 and N5M1 with an orange colour, but the efficiency loss is relatively high due to high reflection in the NIR wavelength range. Increasing M to 3 gives a red colour with moderate lightness and high chroma. In this case, the efficiency loss is smaller due to reduced reflection in the NIR wavelength range. Increasing M to 5 results in a magenta colour.

Fig. 19 displays the Colour Performance Index CPI, defined as Y/P for different N and M. A high CPI value indicates that there is a good trade-off between lightness and efficiency loss. The maximum obtainable CPI value is about 5.5 for a narrow spectral peak at 550 nm [3]. The CPI value of 3.8 for N5M3 and λ_D = 550 nm is close to the maximum possible value for L* = 65. From these results we can conclude that green colours (λ_D = 550 nm) with M = 3 are favourable for achieving a colour with high lightness combined with low efficiency loss, in accordance with the results in [4].

Fig. 20 shows the relative loss P versus chroma. We observe a clear covariation between efficiency and chroma. High chroma with low relative loss can be achieved with λ_D = 450, N = 3, 5 and M = 3, 5, however, these are rather dark colours. In order to obtain high lightness, high chroma, and low relative loss simultaneously, N3M3 and N5M3 for λ_D = 550 nm are favourable.

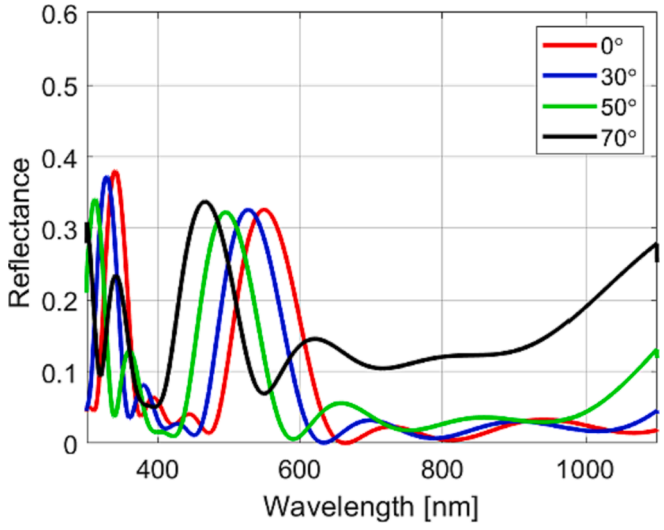

Fig. 13. Simulated reflectance spectra for incidence angles θ_O = 0°, 30°, 50° and 70° for the case N3M3 with low index design (2.0/1.5) and λ_D = 550 nm.

Achieving both low efficiency loss and low angular dependence is challenging. Relative loss vs. maximum colour difference ΔE_{max} is displayed in Fig. 21 and demonstrates that less than 10 % relative loss and ΔE_{max} less than 25 can only be obtained for N = 1. The markers in Fig. 21 also displays the colour, and only dark colours have both low angular dependence and low loss. From Fig. 14 it can also be seen that N = 1 leads to dark colours with low chroma. All designs with high lightness, high chroma, and low relative loss have a high angular colour dependence.

3.5. Design guidelines

Here we present a set of design guidelines that can be used for those who would like to manufacture coloured PV components based on optical interference coatings, with specific visual and/or efficiency properties in mind. The guidelines can also be applied by specifiers such as architects or building owners, that would like to understand the possibilities that interference coatings represent with respect to colouration of PV modules or BIPV components.

3.5.1. High lightness

Many architects and building owners prefer lighter colours on the façade of their buildings. This preference is in stark contrast to the dark appearance that is associated with standard PV modules. From Fig. 17 and from Table 4, we see that only five of the 27 low index cases that have been investigated provide colours with lightness values above 60. These are: 550N5M1 (L* = 78), 550N5M3 (L* = 65), 650N5M1 (L* = 65), 550N3M1 (L* = 63) and 450N5M1 (L* = 61). Note that the numbers 450, 550, and 650 represent the design wavelengths. Increasing N increases lightness significantly for green colours, while that is not always the case for blue and red colours. Also, a design wavelength in the green region (close to 550 nm) generally increases the resulting lightness. This is mainly explained by the high eye sensitivity in this region. If we also, in addition to high lightness, would like to keep the relative loss (P) to a minimum, the case 550N5M3 could be considered.

3.5.2. Low relative loss

In many building projects the energy performance of the PV

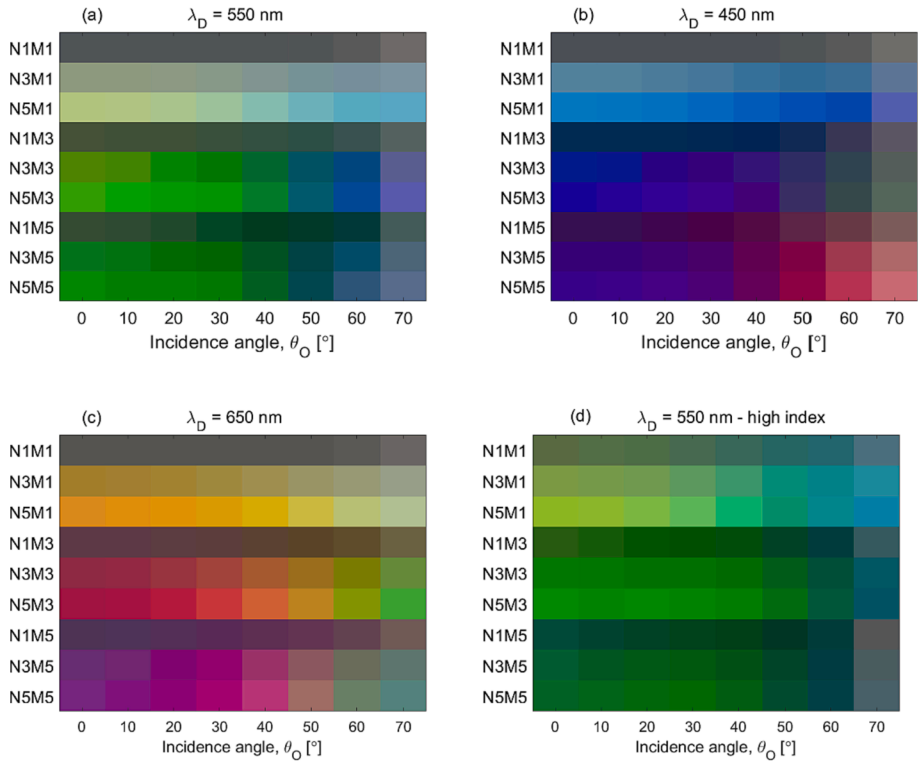

Fig. 14. Colour patches for varying incidence angles θ_O for different N and M. The design wavelength (at 0°) is 550 nm (a) and (d), 450 nm (b) and 650 nm (c). The results are for a low index design (2.0/1.5) (a) - (c), and high index design (2.3/1.8) (d).

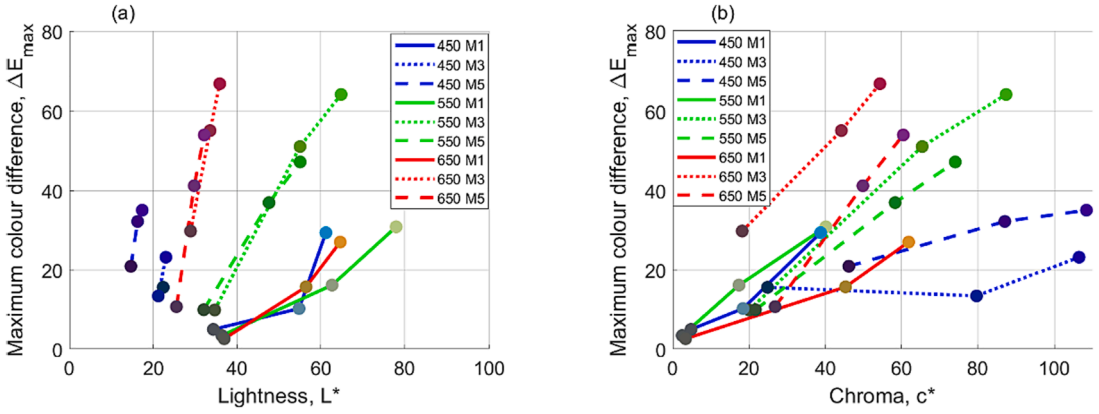

Fig. 15. Maximum colour difference ΔE_{max} versus lightness L* (a) and chroma c* (b). Lines connects results for N = 1, 3, 5. Results are displayed for a low index design (2.0/1.5) and λ_D = 450 nm, 550 nm, and 650 nm.

installation will be a major factor, and keeping the losses associated with colouring at a minimum level will be highly desired. From Fig. 17 and from Table 4, we see that five of the 27 low index cases that have been investigated provide a relative loss (from colouring) that is less than 5%. These are: 550N1M3 (P = 3.5 %), 450N1M3 (P = 3.9 %), 650N1M3 (P = 4.3 %), 650N1M5 (P = 4.8 %) and 450N1M5 (P = 4.9 %). The results show that coating designs with N = 1 should be used when high efficiency is the most important factor. However, the high efficiency comes at the cost of darker colours. When a slightly lighter colour is also desired, the case 550N1M3 could be considered since it combines very low losses (P = 3.5%) with a moderate lightness (L* = 35). Another effect of choosing coating designs with N = 1 is that the angular dependence is generally relatively low for these cases.

3.5.3. *High colour performance index*

A high CPI value indicates that there is a good trade-off between lightness and efficiency loss. This is very relevant for building projects with a desire to apply colours with moderate or high lightness, while still keeping the efficiency as close to the theoretical limit as possible. This can only be accomplished when the reflectance in the NIR is small. From Fig. 19 and from Table 4, we see that four of the 27 low index cases that have been investigated provide a CPI above 2. These are: 550N5M3 (CPI = 3.8), 550N3M3 (CPI = 3.4), 550N5M1 (CPI = 2.3) and 550N1M3 (CPI = 2.0). The results show that coating designs with a design wavelength in the green region (~550 nm) should be used when a high CPI is desired. As noted above, this is mainly explained by the high eye sensitivity in this wavelength region. Also, most of the cases with high CPI applies to M = 3, while M = 5 should be avoided.

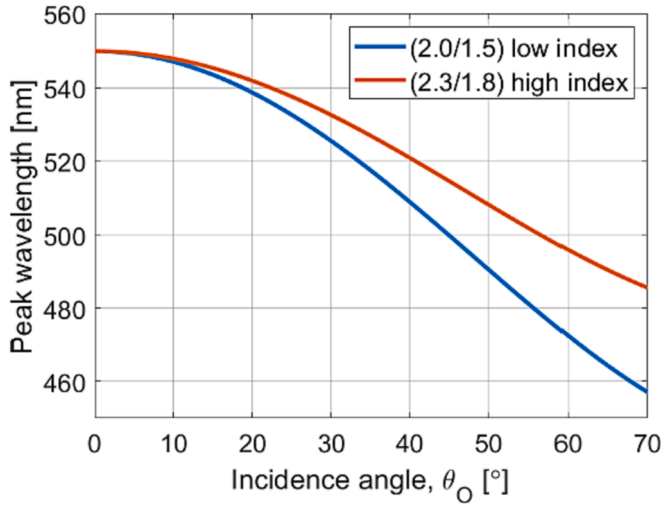

Fig. 16. Calculated interference peak wavelength vs. incidence angle for the low and high index designs in the $\lambda_D = 550$ nm case.

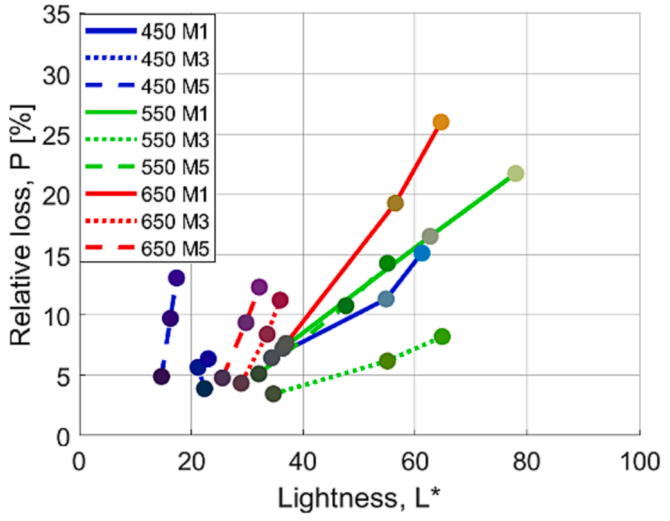

Fig. 17. Relative loss P versus lightness L*. The lines connect results for N = 1, 3, 5. Lowest loss is obtained for N = 1. Results are displayed for $\lambda_D = 450$ nm, 550 nm, and 650 nm.

3.5.4. Low angular dependence

As mentioned in section 3.3. The change of colour with observation angle has been used by architects to create an aesthetic effect. However, most building facades are made of diffusely scattering materials that do not exhibit this property. We therefore assume that most architects or building owners would appreciate colours with a low angular dependence. From Fig. 15 and from Table 4, we see that five of the 27 low index cases that have been investigated provide an angular colour difference ΔE_{max} less than 10. These are: 650N1M1 ($\Delta E_{max} = 2.6$), 550N1M1 ($\Delta E_{max} = 3.4$), 450N1M1 ($\Delta E_{max} = 5.0$), 550N1M3 ($\Delta E_{max} = 9.9$) and 550N1M5 ($\Delta E_{max} = 9.9$). The results show that coating designs with N = 1 and M = 1 provide the smallest angular colour dependence. Note however, that N1M1 provide darker colours with low chroma. When a lighter colour with low angular dependence is desired, the cases of N3M1 could be considered. When high chroma combined with low angular dependence is desired, the case of 450N3M3 (c* = 80 and $\Delta E_{max} = 13.4$) could be considered.

3.5.5. Combination of properties

In many building projects it may be highly desired to combine high power conversion efficiency with certain visual properties. The points below indicate some of the possibilities and challenges in this regard:

- Low efficiency loss combined with low angular colour dependence can only be obtained with N = 1 and results in colours with low or moderate chroma.
- Low efficiency loss combined with high lightness and high chroma can be achieved for green colours ($\lambda_D = 550$ nm) with N3M3 and N5M3.
- Low efficiency loss combined with low angular colour dependence, high lightness and high chroma is a challenge. Here, we again observe that the high index designs perform better than low index designs, especially N1M3 and N3M5.

Regarding combinations of different visual properties, we have also shown that it is possible to obtain low angular colour dependence combined with high lightness or high chroma, but all three of these properties combined is difficult to achieve. One exception is the low index case 650N3M1 (L* = 57, c* = 45 and $\Delta E_{max} = 15.7$). For the high

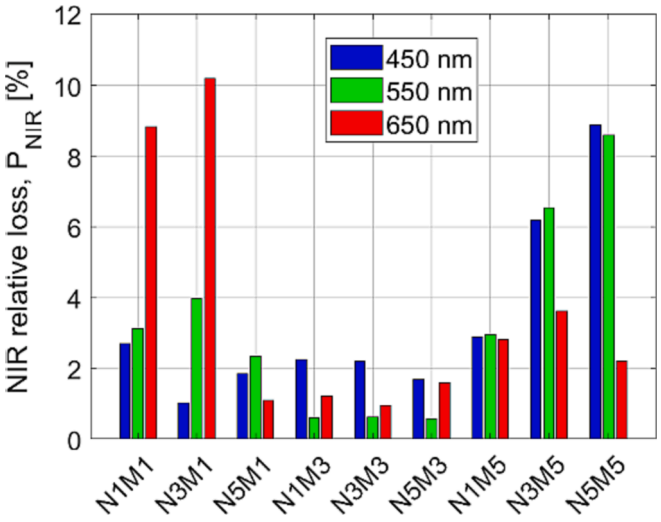

Fig. 18. NIR relative loss P_{NIR} versus layer number N and layer thickness parameter M.

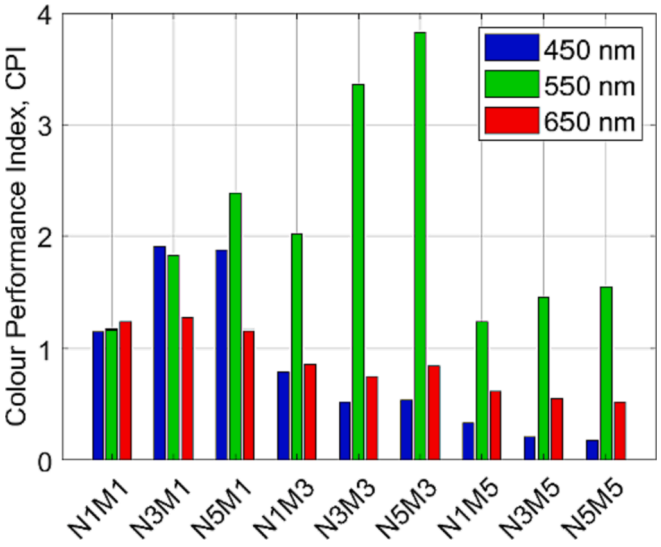

Fig. 19. Colour Performance Index (CPI) versus layer number N and layer thickness parameter M.

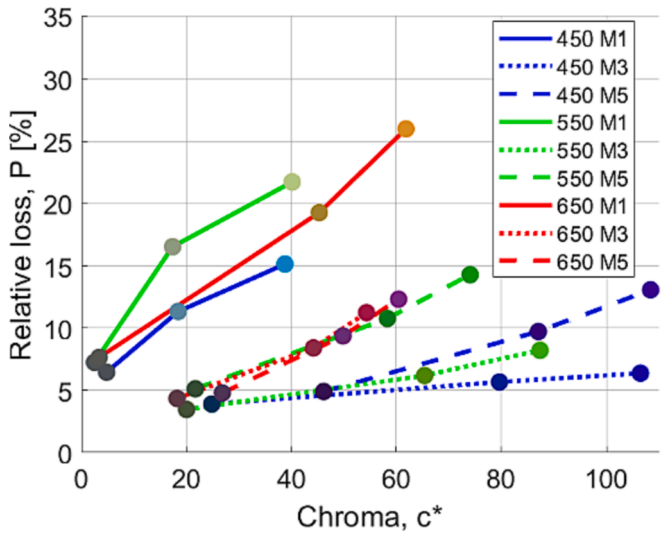

Fig. 20. Relative loss P versus chroma c*. Lines connects results for N = 1, 3, 5 and serve as a guide to the eye. Lowest chroma is obtained for N = 1. Results are displayed for λ_D = 450 nm, 550 nm, and 650 nm.

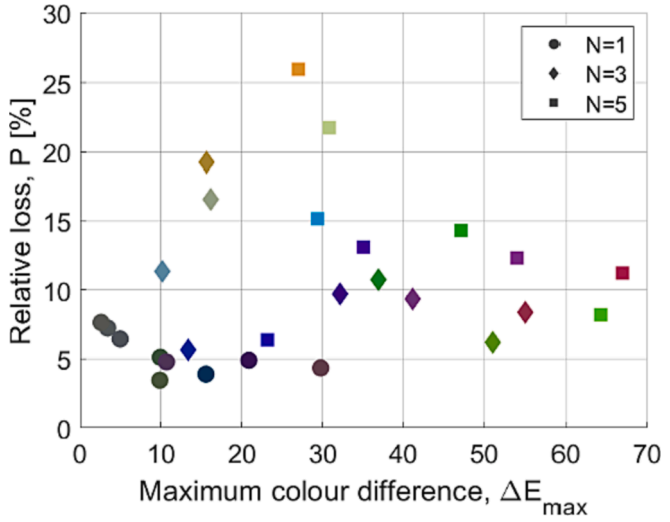

Fig. 21. Relative loss P vs. maximum colour difference ΔE_{max}. The results are for a low index design (2.0/1.5).

index designs, there are more cases that combine high lightness, high chroma and low angular colour dependence.

4. Discussion

In this section, we address some of the limitations of our method, as well as implications of the results. We also introduce and discuss some possibilities for future work on this topic.

In our analysis, we have restricted the values of N and M to 1, 3, and 5, respectively. Increasing N beyond 5 is possible, and will give a stronger interference peak amplitude, while the lightness will not increase noticeably. A disadvantage with high N or M is the increase in the total thickness which may increase fabrication time and cost. Increased thickness may also increase light absorption in the film layers. We have also observed that increasing M from 3 to 5 gives higher NIR losses, and this problem becomes larger with even higher M. In the cases with high N, it is also possible to have non-integer values of M and different M in different layers. This can be used to fine-tune the resulting colour.

Regarding surface roughness, we argue that a small surface roughness will not have a strong impact on efficiency, lightness and chroma, so our findings regarding these properties will be valid also for a typical front glass with a small surface roughness. However, it is not clear exactly how small the roughness must be for the results to be valid, and this remains a topic for further study.

We have included one high index design in the study to illustrate the effect high index has on angular colour dependence. Future work on this will be to expand the study to include more index combinations, and also high index combined with other design wavelengths than 550 nm.

The results from our work could be applied by specifiers such as architects or building owners. As part of our work on this topic, the authors had many discussions with architects regarding aesthetics and the importance of various visual properties for PV modules applied on a building façade.

Architects may desire a specific colour appearance given by a specific combination of L*a*b*. In our work, we did not have any particular emphasis on how a specific L*a*b* combination can be achieved from optical interference coatings. We have analysed how the coating design parameters affect lightness and chroma, but we put much less emphasis on how to obtain a specific hue. The hue is not solely determined by the design wavelength, but also by the combined effect of design wavelength, width of the interference peak, and the spectral overlap with the colour matching functions. A detailed analysis of how to obtain a specific hue or L*a*b* combination is a topic for future work.

Regarding future work, we would also like to see our results explored by researchers looking more closely into the architectural implications of our work. This could for example be done by making scale models of buildings with different types of interference-coloured PV and let architects and lay persons evaluate the architectural implications of the different coating designs. Our new method for quantification of angular colour dependence through the parameter ΔE_{max} was chosen after careful consideration. However, it would be of interest to explore how representative and useful this parameter is with respect to the architectural evaluation of angular colour dependence.

5. Conclusion

In the presented work, we have investigated the use of optical interference coatings for coloured building integrated photovoltaic modules based on crystalline silicon solar cells and analysed the influence of various coating design parameters on the visual properties and efficiency of the photovoltaic modules. The investigation focussed on applying optical interference coating on a planar surface on the back side of the front glass for the photovoltaic module. We found that the experimental results obtained for fabricated samples corresponded well with the results obtained from numerical simulations.

Optical interference coatings typically provide colours that are dependent on the observation angle, and for this reason particular attention was given to the angular dependence of the colours. We have introduced a new parameter for quantification of angular colour dependence, and our results show that the angular colour dependence can be reduced by increasing the refractive indices of the interference coatings.

Based on the results from the numerical simulations, design guidelines that can be used to develop optical interference coatings with certain properties were presented. More specifically, guidelines for achieving high colour lightness, low efficiency loss, high colour performance index, and low angular colour dependence were discussed. For many building projects it may be highly desired to combine high power conversion efficiency with certain visual properties. The results from our work also indicate some of the possibilities and challenges in this regard.

Declaration of Competing Interest

The authors declare that they have no known competing financial interests or personal relationships that could have appeared to influence

the work reported in this paper.

Data availability

Data will be made available on request.

Acknowledgements

The authors thank Bent Thomassen and Junjie Zhu at IFE for technical help in the fabrication of optical interference coatings and the lamination of the experimental samples. The authors also gratefully acknowledge the financial support from the Research Council of Norway through The Research Center for Sustainable Solar Cell Technology (RCN project number 257639).

References

[1] Renewables 2022 – Analysis and forecast to 2027, report by IEA, revised version January 2023, (2023).
[2] C. Ballif, L.E. Perret-Aebi, S. Lufkin, E. Rey, Integrated thinking for photovoltaics in buildings, Nat. Energy 3 (2018) 438–442.
[3] A. Røyset, T. Kolås, B.P. Jelle, Coloured building integrated photovoltaics: Influence on energy efficiency, Energ. Buildings 208 (2020), 109693.
[4] J. Halme, P. Mäkinen, Theoretical efficiency limits of ideal coloured opaque photovoltaics, Energ. Environ. Sci. 12 (4) (2019) 1274–1285.
[5] J. Shih, S-L Lai. H-T. Cheng, The principle and applications of colored solar cells, Advanced Materials Research, (2013), 420-425.
[6] Z. Li, T. Ma, H. Yang, L. Lu, R. Wang, Transparent and colored solar photovoltaics for building integration, Solar RRL 5 (3) (2021) 2000614.
[7] COLOURED BIPV Market, research and development, IEA PVPS Task 15, Report IEA-PVPS T15–07 (2019) 2019.
[8] J.H. Selj, T.T. Mongstad, R. Søndenå, E.S. Marstein, Reduction of losses in colored solar cells with multilayer antireflection coating, Sol. Energy Mater. Sol. Cells 95 (2011) 2576–2582.
[9] M. Li, L. Zeng, Y. Chen, L. Zhuang, X. Wang, H. Shen, Realization of colored multicrystalline cells with SiO2/SiNx: H double layer antireflection coatings, Int. J. Photoenergy 352473 (2013).
[10] L. Zeng, M. Li, Y. Chen, H. Shen, A simplified method to modulate colors on industrial multicrystalline silicon solar cells with reduced current losses, Sol. Energy 103 (2014) 343–349.
[11] K. Ding, X. Zhang, L. Ning, Z. Shao, P. Xiao, A. Ho-Baillie, X. Zhang, J. Jie, Hue tunable, high color saturation and high-efficiency graphene/silicon heterojunction solar cells with MgF2/ZnS double anti-reflection layer, Nano Energy 46 (2018) 257–265.
[12] M. Amara, F. Mandorlo, R. Couderc, F. Gerenton, M. Lemiti, D. Mencaraglia, Temperature and color management of silicon solar cells for building integrated photovoltaic, EPJ Photovoltaics 9 (2018) 1.
[13] M. Rudzikas, A. Setkus, M. Stange, J. Ulbikas, A. Ulyashin, Simple interference based solar cells and panels with ITO/SiNx: H double layer antireflective coatings 207 (2020) 2018–2227.
[14] N. Roosloot, V. Neder, H. Haug, C.C. You, A. Polman, E.S. Marstein, J. Appl. Phys. 129 (2021), 173104.
[15] J. Escarre, H. Y. Li, L. Sansonnens, F. Galliano, G. Cattaneo, P. Heinstein, S. Nicolay, J. Bailat, S. Eberhard, C. Ballif, L. E. Perret-Aebi, When PV modules are becoming real building elements: White solar module, a revolution for BIPV, IEEE 42nd Photovoltaic Specialists Conference (PVSC), (2015).
[16] N. Jolissaint, R. Hanbali, J.-C. Hadorn, A. Schüler, Colored solar facades for buildings, Energy Procedia 122 (2017) 175–180.
[17] T. Karin, A. Jain, Visual characterization of anti-reflective coating on solar module glass, IEEE 47th PVSC (2020).
[18] B. Bläsi, T. Kroyer, T. Kuhn, O. Höhn, The morphocolor concept for coloured photovoltaic modules, IEEE J. Photovoltaics 11 (2021) 1305–1311.
[19] A. Gasonoo, H.-S. Ahn, S. Lim, J.-H. Lee, Y. Choi, Color glass by layered nitride films for building integrated photovoltaic (BIPV) system, Crystals 11 (2021) 281.
[20] A. Wessels, A. Callies, B. Bläsi, T. Kroyer, O. Höhn, Modelling the optical properties of Morpho-inspired thin-film interference filters on structured surfaces, Opt. Express 30 (2022) 14586–14599.
[21] Z. Xu, T. Matsui, K. Matsubara, H. Sai, Tunable and angle-insensitive structural coloring of solar cell modules for high performance building-integrated photovoltaic application, Sol. Energy Mater. Sol. Cells 247 (2022) 111952.
[22] G. Wyszecki, W.S. Stiles, Color Science - Concepts and Methods, Quantitative Data and Formulae, (2nd ed.)., Wiley-Interscience, 2000.
[23] CIE, International commission on illumination, Colorimetry, Technical report, CIE15:2004, 3rd edition,, 2004.
[24] G. Sharma, W. Wu, E.N. Dalal, The CIEDE2000 color-difference formula: Implementation notes, supplementary test data, and mathematical observations, color research & application, Wiley Interscience 30 (1) (2005) 21–30.
[25] H.A. MacLeod, Thin film optical filters, Taylor & Francis, Bristol and Philadelphia, 2001.